Application of a mechanistic UV/hydrogen peroxide model at full-scale: sensitivity analysis, calibration and performance evaluation

W. T. M. Audenaert*,**, Y. Vermeersch*, S. W. H. Van Hulle*, P. Dejans*, A. Dumoulin* and I. Nopens**

* EnBiChem Research Group, Department of Industrial Engineering and Technology, University College West Flanders, Graaf Karel de Goedelaan 5, 8500 Kortrijk
(E-mail: *wim.audenaert@howest.be*; *stijn.van.hulle@howest.be; pascal.dejans@howest.be; ann.dumoulin@howest.be)*
** BIOMATH, Department of Applied Mathematics, Biometrics and Process Control, Ghent University, Coupure Links 653, 9000 Gent
(E-mail: *ingmar.nopens@ugent.be*)

Abstract
Numerous mechanistic models describing the UV/H_2O_2 process have been proposed in literature. In this study, one of them was used to predict the behavior of a full-scale reactor. The model was calibrated and validated with non-synthetic influent using different operational conditions. A local sensitivity analysis was conducted to determine the most important operational and chemical model parameters. Based on the latter, the incident UV irradiation intensity and two kinetic rate constants were selected for mathematical estimation. Hydrogen peroxide concentration, the decadic absorption coefficient at 310 nm (UVA_{310}, as a surrogate for natural organic matter) and pH could be satisfactorily predicted during model validation using an independent data set. It was demonstrated that quick real-time calibration is an option at less controllable full-scale conditions. Parameters that determine the initiation step, i.e. photolysis of hydrogen peroxide, have a large impact on most of the variables. Some reaction rate constants were also of importance, but nine kinetic constants did show absolutely no influence to one of the variables. Parameters related to UV shielding by NOM were of main importance. Hydrogen peroxide concentration was classified as a non-sensitive variable, in contrast to the concentration of a micro pollutant which showed to be very to extremely influential to many of the parameters. UV absorption as a NOM surrogate is a promising variable to be included in future models. Model extension by splitting up the UVA_{310} into a soluble and a particulate fraction seemed to be a good approach to model AOP treatment of real (waste)waters containing both dissolved and particulate (suspended) material.

Keywords
advanced oxidation processes, model calibration, NOM, sensitivity analysis, UV absorption, UV/H_2O_2

INTRODUCTION

The UV/hydrogen peroxide process

The increasing pressure of emerging micro pollutants on the aquatic environment and fresh water resources has resulted in an intensification of scientific research on the sources, fate, effects and removal of these products. Advanced oxidation processes (AOPs) have recently been proven to be very suitable in this context, which has already led to several full-scale applications (Kruithof et al., 2007; Swaim et al., 2008). The driving force of AOPs is the formation of the hydroxyl radical which can virtually oxidize any compound present in the water matrix because of its high oxidation potential (Parsons, 2004). Besides this oxidative power, AOP technologies often simultaneously achieve disinfection and can facilitate the removal of natural organic matter (NOM), which perfectly fits into the multiple-barrier concept often applied at water treatment sites.

Nowadays, research also focuses on the use of AOPs for wastewater treatment and especially the role they can play as integrated tertiary treatment (Kruithof et al., 2007; Hollender et al., 2009;

Bertanza et al., 2010). The use of mathematical models in this context can be of great value for design and optimization purposes. While different models describing the UV/H_2O_2 process were already developed, it is noteworthy that full-scale model studies and implementations are scarce. This can probably be attributed to two major causes: (i) often, research ends at lab-scale and experiments conducted in real natural water are limited, which restricts actual implementation of models at full-scale AOP reactors; (ii) even when very detailed and generally accepted radical pathways are available, the complex reaction mechanism of NOM often impedes the modeling exercise severely which leads to black box approaches that severely limit model performance and applicability. Another important issue is the overparameterisation of models and the lack of sensitivity studies. The latter could shed light on the extent at which model parameters are influencing the model's output variables. Detailed studies regarding this question are scarce, but are very important when performing modeling studies, especially at full-scale.

Modeling the UV/hydrogen peroxide process

Several mechanistic modelling studies were already performed . Glaze et al. (1995) proposed a kinetic model for the UV/H_2O_2 process which was verified using 1,2-Dibromo-3-chloropropane (DBCP) as a model compound. Model predictions agreed well with experimental data, however, scavenging and UV shielding by NOM were not included and experiments were only performed using a well known water matrix. Liao and Gurol (1995) successfully incorporated the influence of NOM by studying the concentrations of n-chlorobutane and hydrogen peroxide in the presence of a known humic acid (HA). Crittenden et al. (1999) significantly improved the earlier model of Glaze et al. (1995) by rejecting the pseudo-steady-state assumptions and including a pH change during the process as a result of acid formation. Further, the effects of NOM could be included although this was not verified as no new experiments were carried out. In the work of Rosenfeldt and Linden (2004), the model was used to predict the degradation of three endocrine disruptors. In this case, hydroxyl radical induced degradation was the dominating destruction mechanism and consequently, scavenging by NOM became more important. The model was verified in synthetic natural water, but also in real natural water, which cannot commonly be found in literature. These researchers highlighted the influencing role of NOM during UV/H_2O_2 treatment and the importance and variability of the dissolved organic carbon (DOC) content.

UV absorption as NOM surrogate

Total organic carbon (TOC) and DOC, expressed in mg (or mole) carbon L^{-1}, are frequently used surrogates for (natural) organic matter (Liao and Gurol, 1995; Sharpless and Linden, 2003; Li et al., 2008). These variables can be easily determined and cover all organic compounds present in the water. However, it is known that using this surrogate has several disadvantages: (1) lumping the whole organic carbon content into one variable implies the use of just one kinetic rate constant in the hydroxyl radical mass balance. However, it has been demonstrated that not all DOC can be classified as NOM and that some waters contain different NOM structures with varying reactivity towards the hydroxyl radical (Westerhoff et al., 1997); (2) in cases where AOPs are integrated in a treatment train and NOM itself is also a target compound to (partially) oxidize (e.g. in drinking water production), models must be able to predict also the concentration and/or structural changes of the organic matter during the treatment. As in these cases the focus is merely to partially oxidize compounds at relatively short hydraulic retention times (HRTs), TOC or DOC do not give a good representation of the reaction progress as they only describe mineralization which mainly occurs at longer reaction times; (3) because of the lack of information provided at short term, the use of TOC or DOC in UV shielding equations is only valid at the beginning of simulations because the amount of shielding can decrease rapidly as the reaction proceeds. This is mainly due to hydroxyl radical attack at reactive double bond sites, which often occurs at a speed which is not proportional to the TOC or DOC reduction. For these reasons, Song et al. (2008) used the decadic UV absorption at

coefficient at 310 nm (UVA_{310}) as a NOM surrogate. This model seemed suitable to use in this study because the interest was to predict NOM concentrations and structural changes during the oxidation process, rather than to follow the concentration of a single organic pollutant in time. An important drawback of UVA measurements however, is that they do not cover the whole organic carbon content, but focus on the olefinic structures containing carbon-carbon double bonds. As such, this surrogate is limited to describe the conversions of only the unsaturated part of the DOC (Westerhoff et al., 1999).

The objectives of this contribution are to: (i) evaluate the performance of a kinetic UV/H_2O_2 model from literature calibrated at full-scale using a real water matrix, (ii) evaluate the usage of the NOM surrogate using non-synthetic influent for different operational conditions, (iii) determine the relative importance of each model parameter through a local sensitivity analysis and (iv) extend the model and discuss further improvements in order to broaden its applicability. Consequently, gaining mechanistic knowledge was the main goal.

MATERIALS AND METHODS

UV/Hydrogen peroxide reactor

A full-scale UV reactor for water reuse at a horticultural industry was used for this study. A schematic representation of the installation is shown in Figure 1. The AOP unit is part of a small wastewater treatment plant consisting of primary sedimentation, biological reed bed filtration, secondary sedimentation, sand filtration, UV/H_2O_2 treatment, granular activated carbon filtration and storage. Surplus crop irrigation water as well as grey and black domestic wastewater are treated.

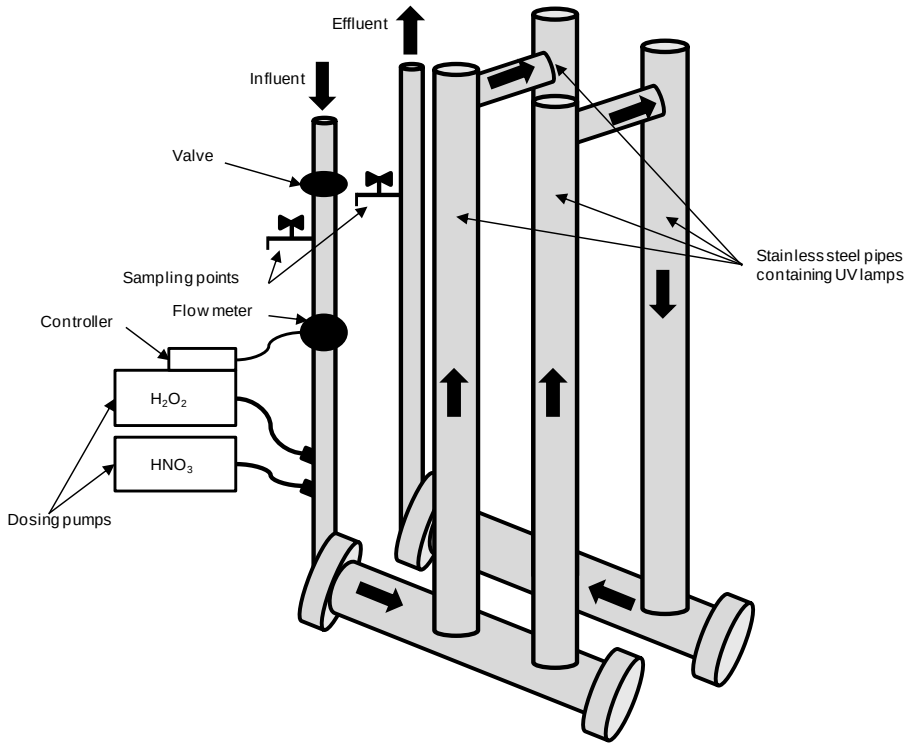

Figure 1: Schematic presentation of the process set-up

The typical influent composition of the UV/H_2O_2 reactor (already primary and secondary treated) is given in Table 1. The AOP reactor consisted of four stainless steel pipes each containing a 205 Watt

low-pressure UV lamp that was 114.5 cm in length (Heraeus, No. NNI 201/107 XL, 480 µW/cm² irradiance at 1m distance) and installed parallel to the water flow. Each lamp was enclosed by a quartz jacket. The total irradiated reactor volume of the four pipes approximated 7.3 L. The influent channel was split into two parts so that each water stream flowed along two lamps in series. The reactor, operating at a nominal flow rate of 2,000 L h^{-1}, was equipped with nitric acid and hydrogen peroxide dosing systems. Nitric acid was used prior to each measurement campaign to rinse the quartz jackets and to prevent scaling of carbonates. The HRT in the reactor was manually adjusted by controlling the incoming water flow with a valve. Flow rates between 120 and 300 L h^{-1} were applied to allow for a sufficient reaction time. Influent samples were taken at a point located just before the hydrogen peroxide dosing pipe. A tap located downstream of the reactor was used to sample the effluent. Samples were taken after a period of three times the HRT to allow the reactor reaching steady-state. Two operational settings were varied during different runs: flow rate (and thus HRT) and hydrogen peroxide concentration.

Table 1: Composition of the reactor influent

Influent parameter	Concentration
pH	7.4-8.2
COD	20-26 mg L^{-1}
TOC	20 mg L^{-1}
UVA_{310}	0.10-0.11 cm^{-1}
UVA_{254}	0.20-0.21 cm^{-1}
Alkalinity	2.6-6.1 mM
Total nitrogen	0.55 mg L^{-1}
Ortho-phosphate	0.70 mg L^{-1}

Modeling approach

Conceptualization. The kinetic model of Crittenden et al. (1999), later modified by Song et al. (2008) was used in this study. However, it should be noted that the simulated data of Song et al. (2008) could not be reproduced. An investigation of the mass balances revealed that a stoichiometric conversion factor to deal with the dissimilarity between the units of UVA (expressed in cm^{-1}) and the hydroxyl radical concentration (expressed in mole L^{-1}) was missing. After adding a factor Y with a numerical value around $1x10^4$ L $mole^{-1}$ cm^{-1} to the mass balance of NOM, the same results could be obtained and the model was ready for use. According to previous models and due to the ease of implementation, the semi- empirical Lambert-Beer law was used to describe the direct photolysis conversion rate. The irradiance (eins s^{-1}) was volume-averaged.

Some adaptations to the model were made. First, NOM photolysis was discarded from the model. Crittenden et al. (1999) stated that degradation of humic substances by direct photolysis could be ignored. This was experimentally verified and indeed, no significant UVA_{310} reduction could be observed. Furthermore, a sensitivity analysis of the original model of Song et al. (2008) classified the parameters with respect to direct NOM photolysis as insignificant (results not shown). Second, the original model was extended by splitting up the the NOM surrogate, UVA_{310}, into two different fractions. UVA_{310} was found to consist of a soluble and a particulate (suspended) fraction, each contributing to UV shielding at 254 nm, but playing different roles in scavenging hydroxyl radicals. This research revealed that the particulate fraction, UVA_{310}^{X}, remained relatively constant during the treatment, and thus only the soluble part, denoted as UVA_{310}^{S}, was assumed to participate in the radical chain. Consequently, for the extended model, two extinction coefficients for NOM at 254 nm, $\varepsilon_{UVA310S}$ and $\varepsilon_{UVA310X}$ (cm^{-1}/cm^{-1}), were used in absorption calculations and hydroxyl radical scavenging by soluble NOM was calculated using one reaction rate constant, k_{16}' ($(1/cm^{-1}).s^{-1}$). For describing UV shielding and radical scavenging with the original model, one molar extinction

coefficient, ε_{UVA310} (cm^{-1}/cm^{-1}), and a rate constant, k_{16} ($(1/cm^{-1}).s^{-1}$), were used, respectively. In both models, a stoichiometric conversion factor Y (L $mole^{-1}$ cm^{-1}) was introduced as discussed earlier. Simulation results of the original and the extended model were compared.
The reaction system is schematically presented in Table 2. In this Gujer matrix [30], the different elementary processes are indicated in the left column. The components shown at the top of the table represent the derived state variables (mole L^{-1}) which have to be calculated with numerical integration. The right column contains the reaction rates of each individual process. The square brackets indicate the concentration of the compound enclosed in the brackets, expressed in mole L^{-1}. Finally, the central matrix elements are stoichiometric factors used in the mass balances. Mass balances can be easily built up by multiplying each matrix element of one column (one variable) by the reaction rate at the same row of the element. A summation of these products yields the conversion terms of the mass balance (Henze et al., 2000). After addition of the transport terms, the complete mass balances can be recovered. A detailed description of composing the mass balances is given in the appendix. This Gujer matrix notation is an elegant way to summarize a set of ordinary differential equations and gives a clear overview of all elementary reactions occurring during the process. More information about the parameters and their values can be found in Table 3.
The fractions of UV radiation absorbed by hydrogen peroxide and a model compound M, respectively, were calculated with the following equations (Song et al., 2008):

$$f_{H_2O_2} = \frac{b \times (\varepsilon_{H_2O_2} \times [H_2O_2] + \varepsilon_{HO_2^-} \times [HO_2^-])}{A} \quad (1)$$

$$f_M = \frac{b \times (\varepsilon_M \times [M])}{A} \quad (2)$$

For the original model, the absorbance of the solution at 254 nm ($A_{254,t}$) was calculated during each time step as follows:

$$A_{254} = b \times (\varepsilon_{H_2O_2} \times [H_2O_2] + \varepsilon_{HO_2^-} \times [HO_2^-] + \varepsilon_{UVA_{310}} \times [UVA_{310}]) \quad (3)$$

For the extended model, Eq. 4 becomes:

$$A_{254} = b \times (\varepsilon_{H_2O_2} \times [H_2O_2] + \varepsilon_{HO_2^-} \times [HO_2^-] + \varepsilon_{UVA_{310}^S} \times [UVA_{310}^S] + \varepsilon_{UVA_{310}^X} \times [UVA_{310}^X]) \quad (4)$$

The dissociation equilibria of carbonates, hydrogen peroxide and hydroperoxyl radicals were described as follows:

$$K_{a_{H2CO3}} = \frac{[H^+] \times [HCO_3^-]}{[H_2CO_3]} \quad (5)$$

$$K_{a_{HCO_3^-}} = \frac{[H^+] \times [CO_3^{2-}]}{[HCO_3^-]} \quad (6)$$

$$K_{a_{H_2O_2}} = \frac{[H^+] \times [HO_2^-]}{[H_2O_2]} \quad (7)$$

$$K_{a_{HO_2^\bullet}} = \frac{[H^+] \times [O_2^{-\bullet}]}{[HO_2^\bullet]} \quad (8)$$

Table 2: Gujer matrix presentation of the reaction system

Process		Components											Reaction Rate
		H_2O_2	•OH	O_2^{-}•	CO_3^{-}•	HCO_3^-	H_2CO_3	M	UVA_{310}	UVA_{310}^S	UVA_{310}^X	TOC	
Photolysis	H_2O_2 (initiation)	-1	2										$\varphi_{H2O2}*I_0*f_{H2O2}*(1-\exp^{(-2,303*A)})$
	M							-1					$\varphi_M*I_0*f_M*(1-\exp^{(-2,303*A)})$
Propagation	$H_2O_2 + •OH$	-1	-1	1									$k_1*[•OH]*[H_2O_2]$
	$HO_2^- + •OH$	-1	-1	1									$k_2*[•OH]*[HO_2^-]$
	$H_2O_2 + O_2^-$•	-1	1	-1									$k_3*[O_2^-•]*[H_2O_2]$
	$H_2O_2 + HO_2$•	-1	1	-1									$k_4*[HO_2•]*[H_2O_2]$
	$H_2O_2 + CO_3^-$•	-1		1	-1	1							$k_5*[H_2O_2]*[CO_3^-•]$
	$HO_2^- + CO_3^-$•	-1		1	-1	1							$k_6*[HO_2^-]*[CO_3^-•]$
Termination	•OH + HO_2•		-1	-1									$k_7*[•OH]*[HO_2•]$
	•OH + HO•	1	-2										$k_8*[•OH]*[•OH]$
	•OH + CO_3^-•		-1		-1								$k_9*[•OH]*[CO_3^-•]$
	•OH + O_2^-•		-1	-1									$k_{10}*[•OH]*[O_2^-•]$
	O_2^-• + CO_3^-•		-1		-1	1							$k_{11}*[O_2^-•]*[CO_3^-•]$
	O_2^-• + HO_2•	1		-2									$k_{12}*[O_2^-•]*[HO_2•]$
	HO_2• + HO_2•	1		-2									$k_{13}*[HO_2•]*[HO_2•]$
	CO_3^-• + CO_3^-•				-2								$k_{14}*[CO_3^-•]*[CO_3^-•]$
	HO• + CO_3^{2-}		-1		1	-1							$k_{15}*[•OH]*[CO_3^{2-}]$
Scavenging	HO• + UVA_{310}^S		-1							-Y	0		$k_{16}'*[•OH]*[UVA_{310}^S]$
	HO• + UVA_{310}		-1						-Y				$k_{16}*[•OH]*[UVA_{310}]$
Micropollutant destruction	HCO_3^- + •OH		-1		1	-1							$k_{17}*[•OH]*[HCO_3^-]$
	•OH + M		-1					-1					$k_{18}*[•OH]*[M]$
Acid formation	•OH + TOC						1					-1	$k_{19}*[•OH]*[TOC]$

Table 3: Parameters of the kinetic model and their values

Parameters		Initial value	Source initial value
Incident light intensity	I_0[a]	6.9 x10^{-5} eins L^{-1} s^{-1}	This work
Optical path length	b	1.2 cm	This work
Second order rate constants	k_1	2.7 x10^7 $M^{-1}s^{-1}$	Buxton et al. (1988)
	k_2	7.5 x10^9 $M^{-1}s^{-1}$	Christensen et al. (1982)
	k_3	0.13 $M^{-1}s^{-1}$	Weinstein and Bielski (1979)
	k_4	2.7 x10^7 $M^{-1}s^{-1}$	Bielski et al. (1985)
	k_5	8 x10^5 $M^{-1}s^{-1}$	Neta et al. (1988)
	k_6	3 x10^7 $M^{-1}s^{-1}$	Neta et al. (1988)
	k_7	6.6 x10^9 $M^{-1}s^{-1}$	Buxton et al. (1988)
	k_8	5.5 x10^9 $M^{-1}s^{-1}$	Buxton et al. (1988)
	k_9	3 x10^9 $M^{-1}s^{-1}$	Holeman et al. (1987) as cited in Song et al., (2008)
	k_{10}	8 x10^9 $M^{-1}s^{-1}$	Neta et al. (1988)
	k_{11}	6.5 x10^8 $M^{-1}s^{-1}$	Eriksen et al. (1985)
	k_{12}	9.7 x10^7 $M^{-1}s^{-1}$	Bielski et al. (1985
	k_{13}	8.6 x10^5 $M^{-1}s^{-1}$	Weinstein and Bielski, (1979)

	k_{14}	2 x10^7 $M^{-1}s^{-1}$	Neta et al. (1988)
	k_{15}	3.9 x10^8 $M^{-1}s^{-1}$	Buxton et al. (1988)
	k_{16} [a]	1.2 x10^4 $(1/cm^{-1})s^{-1}$	Song et al., (2008)
	K_{16}'[a]	1.2 x10^4 $(1/cm^{-1})s^{-1}$	Song et al. (2008)
	k_{17}	8.5 x10^6 $M^{-1}s^{-1}$	Buxton et al. (1988)
	k_{18}	2.2 x10^9 $M^{-1}s^{-1}$	Song et al. (2008)
	k_{19} [a]	4.5 x10^7 $M^{-1}s^{-1}$	Song et al. (2008)
Primary quantum yields for photolysis	φ_{H2O2}	0.5 mole einstein^{-1}[b]	Baxendale and Wilson (1957)
	φ_M	0.14 mole einstein^{-1}[b]	Song et al. (2008)
Molar extinction coefficients	$\varepsilon_{UVA310S}$	2.58 cm^{-1}/cm^{-1}	This work
	$\varepsilon_{UVA310X}$	1,39 cm^{-1}/cm^{-1}	This work
	ε_{UVA310}	2,04 cm^{-1}/cm^{-1}	This work
	ε_M	466.7 $M^{-1}cm^{-1}$	Song et al. (2008)
	ε_{H2O2}	19.6 $M^{-1}cm^{-1}$	Baxendale and Wilson (1957)
	ε_{HO2-}	228 $M^{-1}cm^{-1}$	Baxendale and Wilson (1957)
Equilibrium constants	K_{aH2CO3}	6.3	Crittenden et al. (1999)
	K_{aHCO3-}	10.3	Crittenden et al. (1999)
	K_{aH2O2}	11.6	Crittenden et al. (1999)
	$K_{aHO2\bullet}$	4.8	Crittenden et al. (1999)
Stoichiometric factors	Y	1 x10^4(L $mole^{-1}$ cm^{-1})	This work

[a]these parameters are modified later in this study through parameter estimation
[b]one Einstein equals one mole of photons

Software implementation and numerical solution. The system consisting of 33 parameters, 10 ODEs and 8 algebraic equations was implemented in the generic modeling and simulation platform WEST® (MOSTforWATER, Belgium). Simulations were run in its associated kernel Tornado® (Claeys et al., 2007) which allows to rapidly numerically simulate the stiff system of differential and algebraic equations (DAEs). The stiff solver CVODE (Hindmarsh and Petzold, 1995) was used for all numerical integrations with an absolute and relative tolerance of 1 x10^{-35} and 1 x10^{-5}, respectively.

To simulate the AOP reactor, 25 completely stirred tank reactors (CSTRs) in series were used, according to results of tracer tests (see further). These describe the transport of the water in the system (Froment and Bischoff, 1990). Each reactor contains the complete kinetic model as described above. The configuration as used in the software program is given in Figure 2.

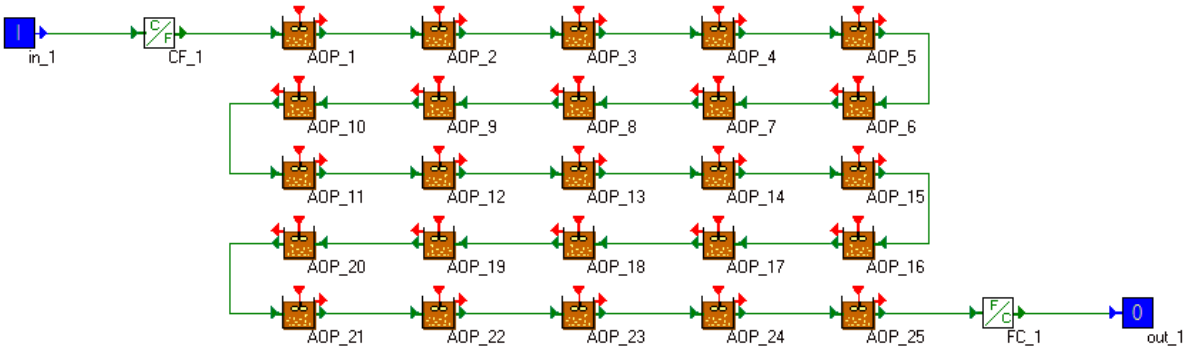

Figure 2: Implementation of the UV/H_2O_2 reactor in the simulation platform WEST®

Model calibration and validation. Three parameters were mathematically estimated: the incident irradiance I_0, k_{16} (k_{16}' in the extended model) and k_{19} (see Tables 2 and 3). The last two parameters are chemical constants related to NOM. The initial value of I_0 was calculated according to the

nominal power input of the lamps (data from the manufacturer), assuming that the LP-UV lamps have an efficiency of 33% (Sharpless and Linden, 2003). Using a factor of 471,652 J Ein^{-1} at wavelength 253.7 nm (Parsons, 2004), a value of $6.9x10^{-5}$ Ein $L^{-1}s^{-1}$ was obtained as initial value. The optical path length was assumed to be equal to the physical path length (1.2 cm) which is the distance between the quartz sleeve and the inner reactor wall and, hence, assumes that all transmitted UV radiation was instantly absorbed by the reactor wall. The extinction coefficient of UVA_{310} was determined by dividing the average influent UVA_{254} by the average influent UVA_{310}.
The Parameter estimation was performed by using the Simplex algorithm provided in Tornado® and simulations were performed as discussed earlier. The variables used to calculate the objective function were the effluent hydrogen peroxide concentration, the UVA_{310}^{S} and pH. The objective function calculation was based on a weighted sum of squared errors (WSSE) between the model predictions and measurements as shown in Eq. 9. Weighting factors were used to prevent discrimination of variables with low numerical values such as UVA_{310}. It can be derived from this equation that objective function calculation was performed for all three variables simultaneously.

$$J(\theta) = \sum_{j}^{3} \sum_{i=1}^{N} w_j (y_{ij} - \hat{y}_{ij}(\theta))^2 \qquad (9)$$

in which $J(\theta)$ represents the objective function based on N data points and y_{ij} and $\hat{y}_{ij}(\theta)$ represent the model prediction and experimental data of variable j, respectively. w_j is the weight factor applied to the variables. Five experimental data points per variable were used in the calibration process. Each data point corresponded to an experimental run with specific operational conditions. Similarly, an independent dataset corresponding to five independent runs was used to validate the model. To investigate changes of the NOM content over time, several months were left between the collection of experimental data for validation and calibration. The dates of data collection together with the influent data and operational conditions that were used for calibration and validation are given in Table 4. Hydrogen peroxide concentrations were chosen according to literature (Glaze et al., 1995; Liao and Gurol, 1995; Crittenden et al., 1999; Sharpless and Linden, 2003; Rosenfeldt and Linden, 2004; Song et al., 2008; Wu and Linden, 2008) and practice.

Table 4: Influent and operational conditions used for calibration and validation data collection

Calibration run No.	Date	Flow rate ($L\ s^{-1}$)	HRT (s)	$[H_2O_2]$ (mM)	$[HCO_3^-]$ (mM)	$[UVA_{310}]$ (cm^{-1})	$[UVA_{310}^{S}]$ (cm^{-1})	$[UVA_{310}^{X}]$ (cm^{-1})	[TOC] (mM)	SUVA ($cm^{-1}\ M^{-1}$)	pH
1	10/06/2010	0.077	95	0.7	4.46	0.108	0.056	0.052	1.7	0.0105	7.49
2	10/06/2010	0.077	95	1.1	4.46	0.109	0.059	0.050	1.7	0.0108	7.59
3	10/06/2010	0.077	95	1.8	4.41	0.108	0.060	0.048	1.7	0.0108	7.54
4	10/06/2010	0.077	95	2.7	4.41	0.108	0.060	0.048	1.7	0.0108	7.58
5	10/06/2010	0.077	95	4.0	4.41	0.107	0.059	0.048	1.7	0.0109	7.54
Validation run No.											
1	03/12/2009	0.086	85	1	2.59	0.112	0.051	0.061	1.9	0.0097	7.39
2	03/12/2009	0.086	85	3.8	2.59	0.101	0.046	0.055	1.9	0.0089	7.39
3	28/04/2010	0.035	212	0.48	6.172	0.127	0.070	0.057	2.0	0.0095	8.16
4	28/04/2010	0.035	212	1.65	5.987	0.118	0.061	0.057	2.9	0.0062	8.13
5	28/04/2010	0.035	212	2.34	6.099	0.118	0.058	0.060	2.4	0.0075	8.12

Goodness-of-fit test. During each simulation run, the system was allowed to stabilize and the corresponding steady state values were used to compare with the experimental data from the effluent. The goodness-of-fit between experimental and simulated values for a variable using the

optimized parameters was quantified by calculating Theil's inequality coefficient (TIC) according to Audenaert et al. (2010). A value of the TIC lower than 0.3 indicates a good agreement with measured data (Audenaert et al., 2010).

Experimental methods

Analytical procedures. All samples were collected in glass bottles and immediately brought to 2°C using ice. Small aliquots of effluent samples for hydrogen peroxide analysis were adjusted to pH 4 using sulfuric acid. In this way, spontaneous hydrogen peroxide loss during transportation was prevented. The remainder of the effluent samples were stored as such for all other analysis. Although a relatively constant influent composition could be expected, an influent sample was taken at the beginning of each individual experimental run.

Hydrogen peroxide concentrations were determined using the iodide/iodate method of Klassen et al. (1994). Prior to all other analysis, hydrogen peroxide was removed by adding small amounts of freshly prepared sodium sulphite solution to the stirred samples at room temperature. Influent hydrogen peroxide was determined by switching off the UV lamps and determining the effluent concentration using the same procedure as outlined above.

UV absorption measurements were performed in 1-cm path-length quartz cuvettes using a Shimadzu UV-1601 spectrophotometer. Of each influent and effluent sample, a part was filtered using a prewashed 0.45 µm PTFE filter to determine the soluble fraction of UVA_{310} (UVA_{310}^{S}). The particular fraction, UVA_{310}^{X}, was determined by subtracting UVA_{310}^{S} from the total UVA_{310}. A Shimadzu TOC-VCPN analyzer was used to measure the TOC. pH was monitored using an Ecoscan pH5 apparatus (Eutech Instruments). Alkalinity was determined according to Standard Methods (1992).

Tracer test. To mimic the hydraulic behaviour of the AOP reactor, a tanks-in-series (TIS) approach was used. A tracer test (Froment and Bischoff, 1990) was performed to determine the number of CSTRs to be used in the simulation software. A pulse of 10 ml sodium chloride (10 %) was rapidly injected into the hydrogen peroxide addition port. On-line conductivity measurements at the effluent sampling valve were used to record the salt concentration residence time distribution (as sodium chloride concentration is directly correlated to conductivity). The tracer test was performed at three different flow-rates to study the effect of the liquid velocity on the mixing properties. The tested flow-rates were 1000, 350 and 120 L h^{-1}. Through comparison of the experimentally obtained dimensionless hydraulic residence time distributions (E(t')) and the theoretical computed ones, the optimal number of tanks (n) was determined according to Froment and Bischoff (1990).

As mentioned in earlier, the irradiated reactor volume approximated 7,3 L. Nevertheless, this volume could not be used in the calculations, because the reactor volume between the point of tracer injection and conductivity measurement contained extra, non-active reactor parts (see Figure 1). The total volume measured with the tracer test was calculated to be 11 L, which was a realistic value.

Sensitivity analysis. To allow comparison between sensitivity functions (SFs) of different variable-parameter combinations, relative sensitivity functions (RSFs) were used (Audenaert et al., 2010) rather than absolute SFs. All simulations were run using the Tornado® kernel (backend of the WEST modeling and simulation platform) and the steady-state RSF values were calculated using the optimized parameters. An additional organic compound (M) with known reactivity towards the hydroxyl radical was included in this experiment to study the parameter sensitivity of micro pollutants during model predictions. The synthetic organic compound alachlor was used for this purpose (Song et al., 2008). The RSF was calculated from the absolute sensitivity function (ASF) using the finite forward difference method with a perturbation factor of $1x10^{-6}$ (Audenaert et al., 2010). A RSF less than 0.25 indicates that the parameter is not influential. Parameters are

moderately influential when 0.25<RSF<1. When 1<RSF<2 and RSF>2, the parameter seems to be very and extremely influential, respectively (Audenaert et al., 2010) (and references therein). The sign of the RSF value specifies if raising the parameter impacts the variable in a positive (higher variable value) or negative (lower variable value) way. The extended model was used to perform the sensitivity analysis.

RESULTS AND DISCUSSION

Tracer Test

For all three flow rates tested, a value of 25 TIS was the final outcome, indicating not well-mixed conditions. As such, this number was used in the simulation configuration depicted in Figure 2 with each reactor having the same volume (V_n) of 0.44 L. Four non-irradiated tanks at the beginning and at the end represented the dark reactor parts, with the irradiance set to zero. Hence, the active reactor part was represented by 17 of the 25 tanks. Preliminary experiments revealed that increasing the number above 15 no longer significantly affects the steady-state output concentrations. This sensitivity check indicated that the number of 17 could be used without expecting significant errors. In the irradiated tanks, the estimated irradiance was used.

Model calibration

The rationale for extending the model can be explained using Figure 3. This figure shows that the particulate fraction of UVA_{310} is not affected by AOP treatment and only the soluble part is oxidized and thus responsible for UVA_{310} decrease. The conditions corresponding to each run number (indicated on the x-axis) are presented in Table 4. UVA_{310} rapidly decreases as the applied hydrogen peroxide concentration is increased up to 2.7 mM (run No. 4). Beyond this concentration (run No. 5), the remaining UVA_{310} remains unchanged at a value of 0.070 cm^{-1}. It is hypothesised that at this concentration hydrogen peroxide itself becomes an important scavenger for hydroxyl radicals. Song et al. (2008) in their studies used the synthetic organic chemical alachlor and showed a stabilization of the observed pseudo-first-order rate constant between 2 and 3 mM hydrogen peroxide.

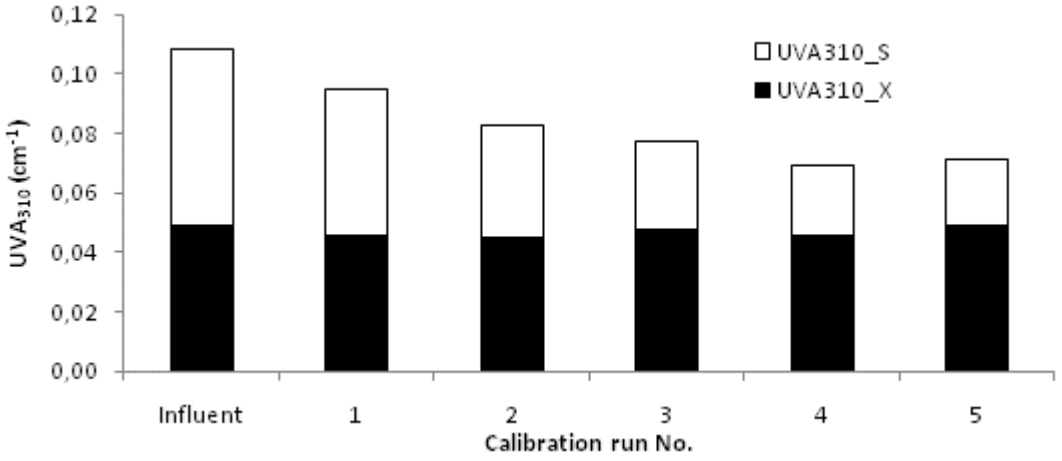

Figure 3: changes of UVA_{310} composition due to AOP treatment during the calibration runs

Calibration results for UVA_{310} are depicted in Figure 4. Low TIC values (0.009 for the original and 0.013 for the extended model) revealed that an excellent agreement was obtained between calculated and experimental data for both models. The value of k_{16}, the second order rate constant for reaction between the *OH radical and UVA_{310} in the original model, was estimated to be 17,138 $(1/cm^{-1})s^{-1}$. This value is in the same order of magnitude but significantly higher than the value of

12,000 $(1/cm^{-1})s^{-1}$ experimentally determined by Song et al. (2008). This illustrates the variable character and related reactivity of organic matter, even within the class of olefinic structures (associated with UVA measurements). Westerhoff et al. (1999) highlighted the importance of molecular weight and other characteristics with respect to *OH radical attack. Rate constant k_{16}' related to hydroxyl radical scavenging of UVA_{310}^{S} in the extended model was estimated to be 34,498 $(1/cm^{-1})s^{-1}$. It was expected that this value would be approximately twice the value of k_{16} of the original model since the influent total UVA_{310} consists of about 50% UVA_{310}^{S} (see Figure 4).

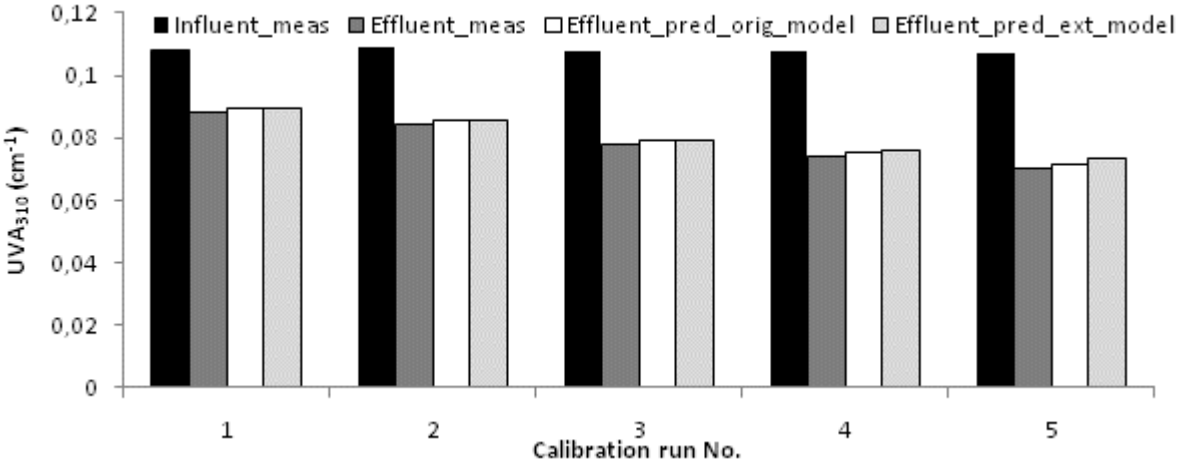

Figure 4: Measured and predicted UVA_{310} after model calibration

Measured and predicted hydrogen peroxide concentrations are presented in Figure 5. The error bars correspond to the 95% confidence interval of three replicate measurements. Simulation outputs of the two models were not presented separately as the results obtained were almost identically.

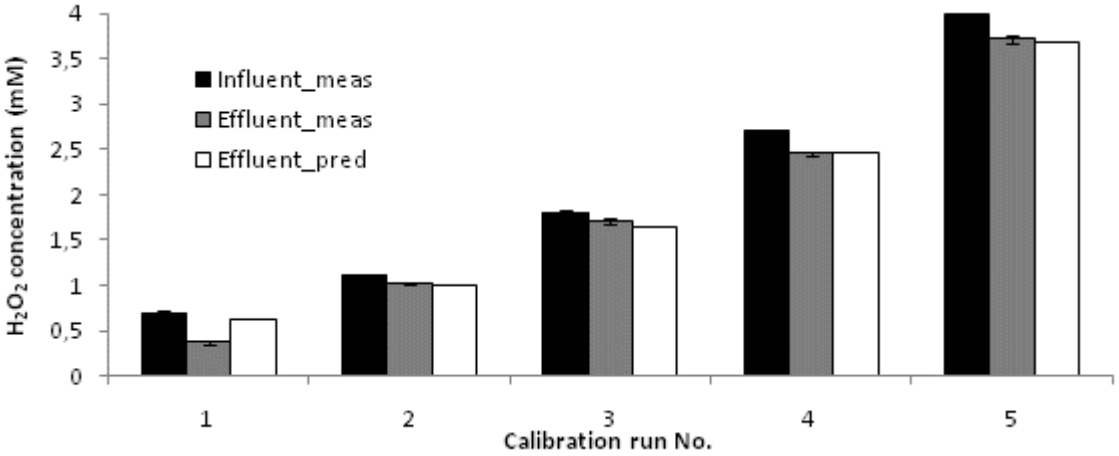

Figure 5: Measured and predicted H_2O_2 concentration after model calibration

It can be clearly observed that the effluent hydrogen peroxide concentration could be accurately predicted, resulting in a very low TIC value (0.028). Based on the sensitivity analysis (see further), I_0 was the most important fitting parameter with respect to this variable. I_0 was estimated to be 2.96 $x10^{-5}$ eins L^{-1} s^{-1} for the original model and 2.92 $x10^{-5}$ eins L^{-1} s^{-1} for the extended version. These values are about 50% lower than the theoretical initial value. However, the initial value (acalculated earlier) assumed that all emitted radiation reached the solution. Most likely, effects such as lamp aging, scaling and sleeve absorption are the underlying reasons for this finding. Sharpless and Linden (2003) estimated the attenuation caused only by the quartz sleeve at 10%. Li et al. (2008)

took into account a UV irradiation decrease of 30% caused by scaling and lamp aging. Probably, sleeve absorption, (irreversible) scaling and lamp aging all contributed to a lower incident UV irradiation.
The calibration results of the solution pH are given in Figure 6. NOM oxidation slightly affects the pH with a pH drop ranging between 0 and 0.11. Model predictions were very satisfactory with a calculated TIC of 0.002 (for both models).

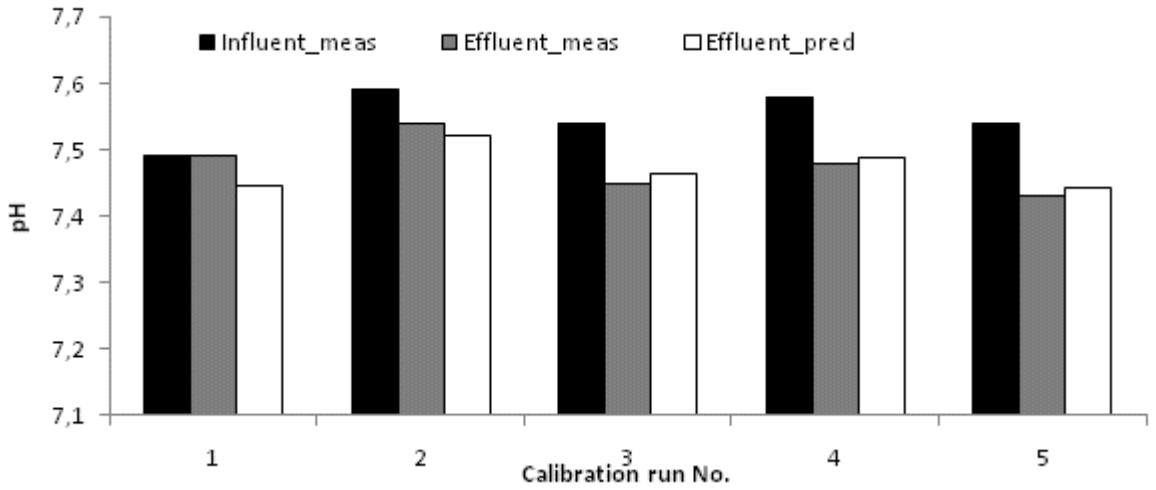

Figure 6: Measured and predicted pH after model calibration

Model validation
Validation results for the UVA_{310} are shown in Figure 7. This graph indicates a successful validation. Very low TIC values of 0.056 and 0.052 for the original and extended model, respectively, confirmed the good agreement between experimental and calculated data. Based on TIC, the extended model thus gives a slightly better result which is, however, proven to be not not statistically significant using an F-test (Kletting and Glatting, 2009). These data were collected at least four months before the data for calibration (and data of run No's 1 and 2 with another two weeks difference). The deviations between experimental and predicted data are most likely a result of a changing NOM content and its complex reaction mechanism. The specific UV absorption coefficient at 254nm ($SUVA_{254}$, (mg C/L^{-1})cm^{-1}) which is calculated by dividing the UVA_{254} by the TOC concentration (in mg L^{-1}) is often related to the reactivity of NOM (Westerhoff et al., 1999). The mean SUVA of the influent during the calibration experiments was around 0.0108 (mg C/L^{-1})cm^{-1} while that of the validation runs was approximately 20% less. SUVA values and dates of data collection are given in Table 4.

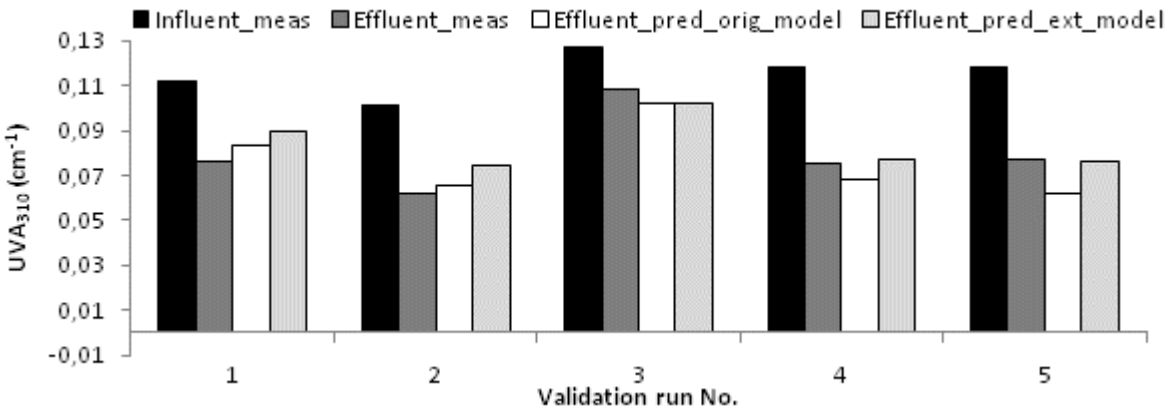

Figure 7: Measured and predicted UVA_{310} in the validation process

Rosenfeldt and Linden (2004) recognized the complexity of performing modelling studies in the presence of an unknown NOM matrix. Several factors that can influence the reaction rate are not included in the model. pH may affect the reactivity of the humic acid part of the DOC content. The reactivity of the deprotonated and thus negatively charged form is usually higher than that of the protonated form because of the decreased nucleophilicity (von Gunten, 2003). However, this effect is probably of less importance as only minor changes in pH were observed during all experiments (see further). Moreover, a part of NOM acts as direct radical scavenger, while another fraction can act as a chain promoter (Westerhoff et al., 1997). Another issue that may affect the UVA_{310}^{S} concentration profile is the formation of oxidation by-products that have a higher extinction coefficient at 254 nm than the parent compound. Glaze et al. (1992) showed that during the oxidation of naphthalene naphthols and quinones are formed, which have higher absorptivities than naphthalene. Hence, a stabilization of UVA was observed during prolonged oxidation. The validation results suggest that UVA_{310} is a promising variable to be part of future and more complex models but more studies are needed to further improve the predictions.
Validation results for hydrogen peroxide are depicted in Figure 8. Again, simulation outputs of both models were not presented separately as these results were almost identically.

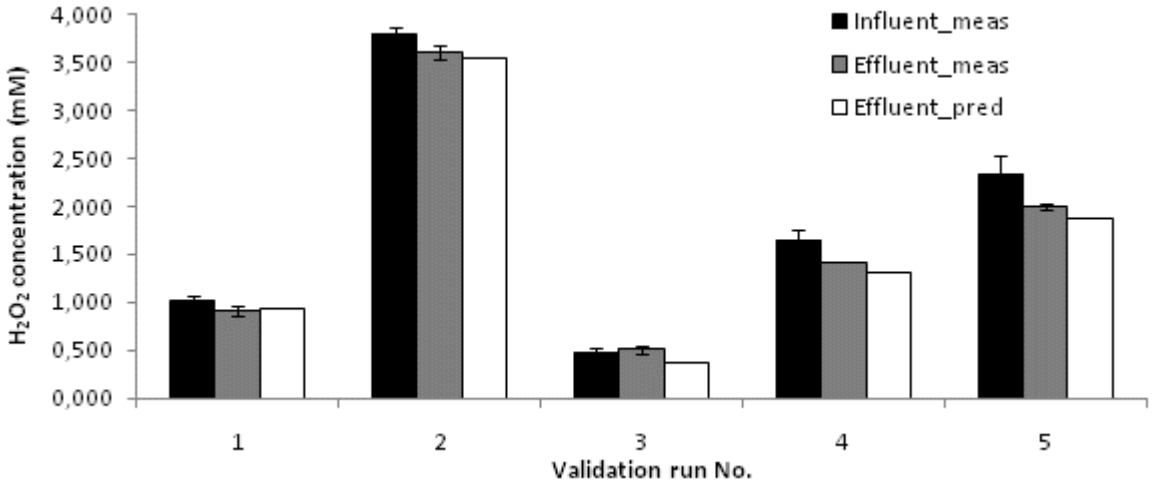

Figure 8: Measured and predicted H_2O_2 concentration in the validation process

Bearing in mind the excellent calibration results, the hydrogen peroxide concentration was expected to show good predictions during validation. Indeed, the residual hydrogen peroxide concentration was described very well by the model, with a resulting TIC value of 0.026. However, a slight underestimation of the H_2O_2 concentration can be observed. Although the UVA_{310} extinction coefficients showed some time-related variations, they are unlikely to significantly influence the hydrogen peroxide conversion as they can be classified as not influential with regard to this variable (see further in section 3.4.).
The validation results for pH are presented in Figure 9. For the same reason as mentioned above, simulation outputs of both models were presented by just one bar. A satisfactory model prediction was obtained (TIC=0.01). The shape of the calculated curve describes the general trend of the experimental data points very well. The influent pH of run Nos 3 to 5 is relatively high compared to all others, which explains the more drastic pH drops during AOP treatment (as pH is a logarithmic scale). However, the model significantly underestimates the acid formation of these runs. This can be a result of time-related changes of TOC characteristics with respect to reactivity (the variability of SUVA was discussed earlier).

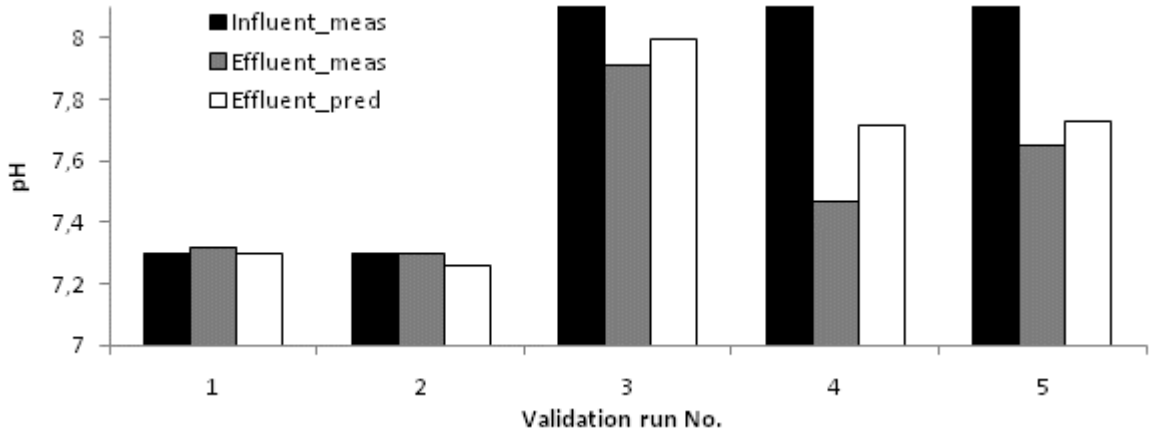

Figure 9: Measured and predicted pH in the validation process

Sensitivity analysis

An important goal of this study was to quantify the influence (i.e. importance) of each model parameter with respect to all output variables. As such an analysis results in a large amount of information, only the most remarkable outcomes were graphically presented and/or discussed. The influent characteristics of calibration run No. 3 (see Table 4) extended with an additional micro pollutant (M) were used in this analysis. This run was chosen because of the intermediate applied hydrogen peroxide concentration. The concentration of M ([M]) was chosen to be 1 µM. The sensitivity of the key variables [UVA_{310}^{S}], [*OH], A and [M] to four kinetic rate constants is presented in Figure 10. This figure illustrates to what extent hydroxyl radical scavengers influence the UV/H_2O_2 process. Kinetic rate constants k_1 and k_{17}, describing scavenging by hydrogen peroxide and bicarbonate ions, respectively, are found to be very important. The same parameters are, however, only moderately influential to the UVA_{310}^{S} and the hydroxyl radical concentration. Contrarily, the effect of these parameters on micro pollutant concentrations is even higher with RSF values indicating a major impact (RSF>1) (Audenaert et al., 2010) (and references therein). Also noteworthy is that in this case, increasing the hydrogen peroxide scavenging rate has a larger impact on the process performance compared to altering scavenging by bicarbonate. Scavenging by carbonate ions seems to be of less importance, at least in the pH range studied here, as k_{15} (not included in this graph) was classified as a non-influential parameter. Rate constant k_{16}' has a moderate impact on UVA_{310}^{S} and absorbance at 254 nm. This can be easily explained by the fact that this rate constant is directly related to UVA_{310} reduction. Increasing this value results in a lower effluent UVA and hence, a lower absorbance. It is remarkable that k_{16}' also exerts a negative influence on the concentration of M (which means that with a higher value of k_{16}', a lower micro pollutant concentration could be achieved), although this rate constant is related to a scavenging process. This reveals that competitive radiation absorption by NOM is more detrimental than its reaction with OH radicals regarding micro pollutant removal. Kinetic constant k_{10} is only moderately affecting [M] and has a minor impact on all other variables. The latter, however, may highlight the need for extension of future models with equations describing NOM as a chain promoter (producing superoxide radicals) in order to reliably predict micro-pollutants decay in a real water matrix. Additionally, this parameter has widespread reported literature values ranging between 7 $x10^9$ and 1 $x10^{10}$ (Glaze et al., 1995; Einschlag et al., 1997; Crittenden et al., 1999; Fabian, 2006; Song et al., 2008), indicating that the process description in the model is likely not adequate. This finding illustrates the importance of including uncertainty analysis in the modelling exercise in order to quantify the reliability level of future models. Furthermore, Figure 10 shows that the RSF pattern of the *OH radical concentration is the opposite of that of organic pollutants (NOM and M). This is easy to understand as effluent pollutant concentrations are inversely correlated to the hydroxyl radical concentration. Similarly, Figure 11 describes the influence of

other important operational and chemical parameters. Here, the importance of parameters related to hydrogen peroxide photolysis surfaces. φ_{H2O2}, ε_{H2O2} and I_0 have a very high impact on the hydroxyl radical concentration. This sensitivity is directly reflected in moderate impacts on the UVA_{310}^{S}. Increasing the hydrogen peroxide extinction coefficient involves a higher hydroxyl radical production and hence, a lower final NOM concentration. Although the absorption of hydrogen peroxide increases, the absorbance at 254 nm is negatively influenced. This can be explained by the important role NOM plays in eq. 4. Analogically, an increment of NOM extinction coefficients leads to the opposite effects. and extreme impacts on the concentration of M (Figure 12). The extinction coefficients of NOM seem to be only influential to the concentration of M, and this to a moderate level.

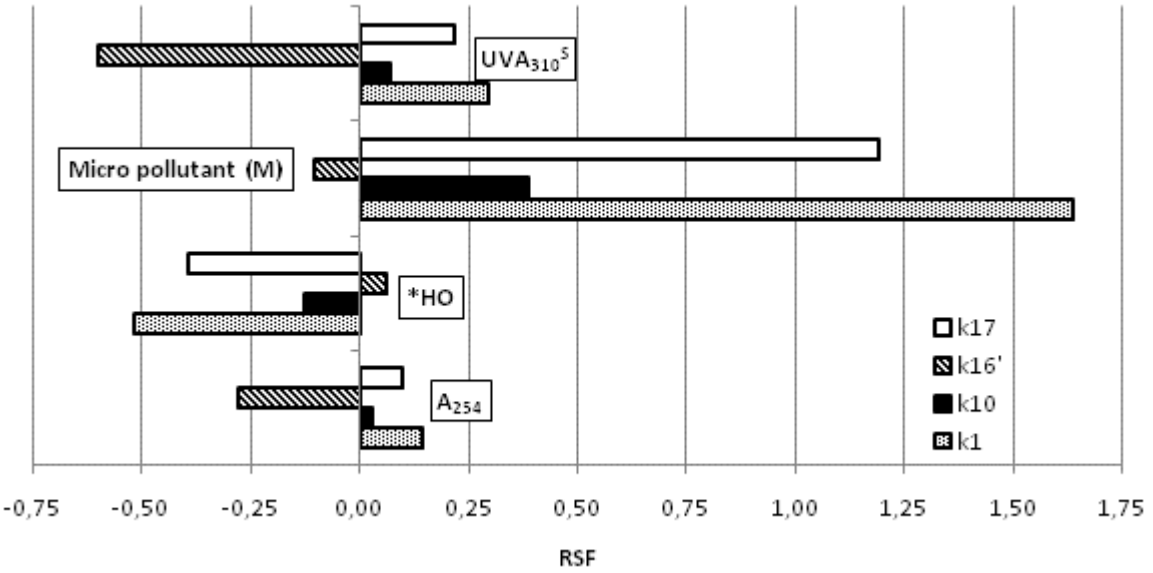

Figure 10: Sensitivity of [UVA_{310}^{S}], [M], [*OH] and $A_{254,t}$ to influential rate constants

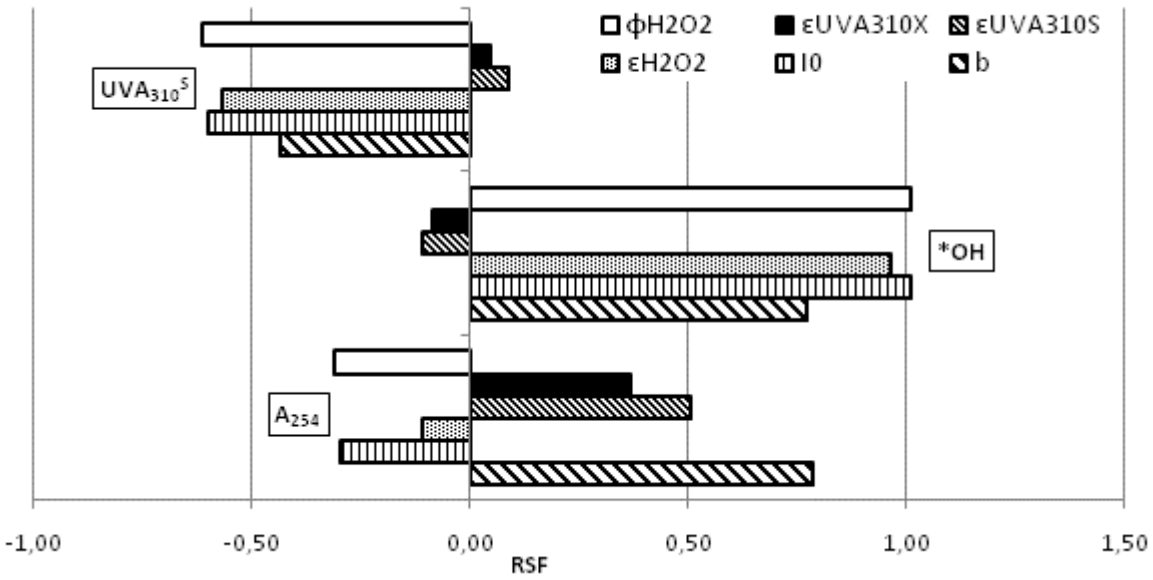

Figure 11: Sensitivity of [UVA_{310}^{S}], [*OH] and $A_{254,t}$ to influential physical and chemical parameters

It becomes clear from Figure 12 that concentrations of micro pollutants (in this case alachlor as

example) are very sensitive to some of the rate constants and extremely sensitive to most of the process parameters. Regarding this sensitivity to the model parameters, one thus has to consider determination of parameters as an important and delicate issue, whether these parameters are being experimentally or mathematically determined, in order to predict these (low) concentrations in a reliable way. In contrast, hydrogen peroxide can be classified as an insensitive variable. Only the parameters associated to direct H_2O_2 photolysis such as I_0, b, ε_{H2O2} and φ_{H2O2} have a little (negative) effect on this variable with RSF values around -0.10.

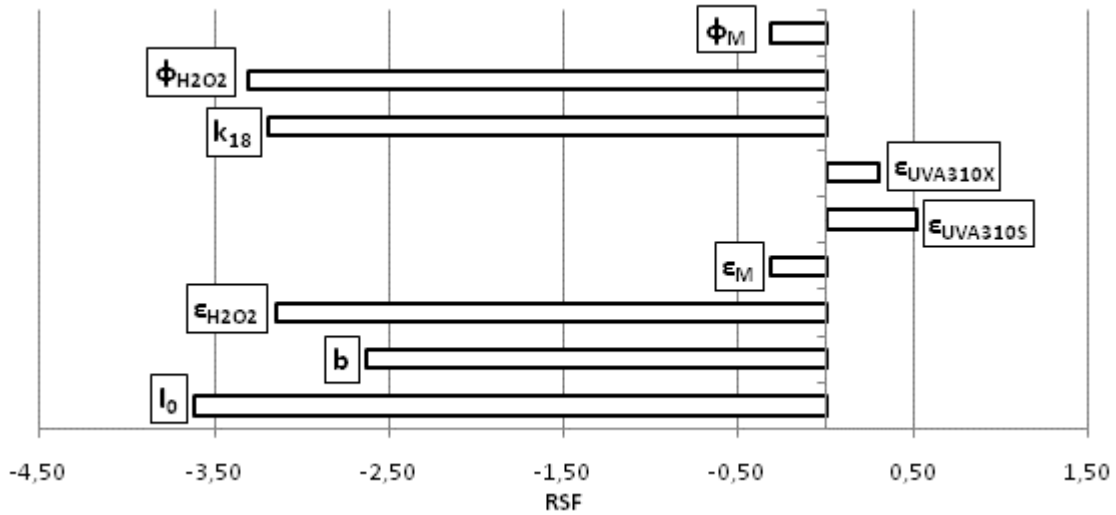

Figure 12: Influence of process and chemical parameters on the prediction of a micro pollutants concentration [M]

Nine rate constants showed to exert absolutely no influence to all of the variables: k_2-k_4, k_6-k_9 and k_{13} and k_{14}. Fábián (Fabian, 2006) mechanistically modeled ozone decomposition in the presence of hydrogen peroxide and removed some of these kinetic parameters. Also in this study, the reliability of the handful of literature reported kinetic parameters was questioned. They were therefore determined by mathematical parameter estimation.

CONCLUSIONS

Mechanistic modeling of organic matter conversions during AOP treatment is one of the current research challenges. Although these mechanisms are often very complex and highly time and case dependent, completing this exercise is essential in order to provide models that are widely applicable and can be used for system optimisation and process control. In this study, an existing UV/H_2O_2 model containing a general accepted radical mechanism was calibrated and validated using data of a full-scale reactor treating non-synthetic influent. It was shown that using the decadic absorption coefficient at 310 nm is a useful variable to include in AOP models. Both the models were able to describe the residual hydrogen peroxide concentration, NOM conversions in terms of UVA_{310} and acid formation resulting in pH drops. The models were successfully validated. Model extension by splitting up the UVA_{310} into a soluble and a particulate fraction seemed to be a good approach to model AOP treatment of real (waste)waters containing both dissolved and particulate (suspended) material. Based on TIC, predictions of the extended model were slightly better than those of the original model but differences were not statistically significant. Hence, further model development, has to focus on understanding and effectively extending the concept of (natural) organic matter conversion. A small attempt to extend an existing model was made in this study. To build these more complex models, more advanced measurement techniques should be used that

provide more detailed information about the characteristics of the organic matrix such as mass spectrometry and polarity measurements. On-line spectral measurements could be of great value in this context as they often supply a large amount of (reliable) data. Future AOP models should also incorporate parameter and input uncertainty to quantify their output uncertainty. This is a very important issue with respect to full-scale applications.

Making models more complex at one side might be performed in parallel with simplifying the models at the side of the radical mechanism in order to balance the model complexity. Model simplification will be part of future research but was beyond the scope of this work. This study revealed that the UV/H_2O_2 process is highly affected by just a fraction of the operational and chemical parameters. Parameters that determine the initiation step, i.e. photolysis of hydrogen peroxide, are very influential to most of the variables. Some reaction rate constants, however, were also of importance. Residual hydrogen peroxide concentration could be classified as a non-sensitive variable. This is in contrast with the extreme sensitivity of micro pollutant concentrations to most of the process parameters. In order to predict these in a reliable way, one thus has to consider determination of parameters as an important and delicate issue, whether these parameters are being experimentally or mathematically determined.

ACKNOWLEDGEMENTS

The authors gratefully acknowledge Hans Pattyn of the V.T.I.-VSBBO Poperinge for the cooperation and making the sampling campaign possible. This research was partially funded by a University College West Flanders PhD research grant and is in close cooperation with the Veg-i-Trade FP7-KBBE-2009-3 project.

REFERENCES

Audenaert, W. T. M., Callewaert, M., Nopens, I., Cromphout, J., Vanhoucke, R., Dumoulin, A., Dejans, P., and Van Hulle, S. W. H. (2010). Full-scale modelling of an ozone reactor for drinking water treatment. *Chemical Engineering Journal* **157**, 551-557.

Baxendale, J. H., and Wilson, J. A. (1957). THE PHOTOLYSIS OF HYDROGEN PEROXIDE AT HIGH LIGHT INTENSITIES. *Transactions of the Faraday Society* **53**, 344-356.

Bertanza, G., Pedrazzani, R., Zambarda, V., Dal Grande, M., Icarelli, F., and Baldassarre, L. (2010). Removal of endocrine disrupting compounds from wastewater treatment plant effluents by means of advanced oxidation. *Water Science and Technology* **61**, 1663-1671.

Bielski, B. H. J., Cabelli, D. E., Arudi, R. L., and Ross, A. B. (1985). REACTIVITY OF HO2/O-2 RADICALS IN AQUEOUS-SOLUTION. *Journal of Physical and Chemical Reference Data* **14**, 1041-1100.

Buxton, G. V., Greenstock, C. L., Helman, W. P., and Ross, A. B. (1988). CRITICAL-REVIEW OF RATE CONSTANTS FOR REACTIONS OF HYDRATED ELECTRONS, HYDROGEN-ATOMS AND HYDROXYL RADICALS (.OH/.O-) IN AQUEOUS-SOLUTION. *Journal of Physical and Chemical Reference Data* **17**, 513-886.

Christensen, H., Sehested, K., and Corfitzen, H. (1982). REACTIONS OF HYDROXYL RADICALS WITH HYDROGEN-PEROXIDE AT AMBIENT AND ELEVATED-TEMPERATURES. *Journal of Physical Chemistry* **86**, 1588-1590.

Claeys, F. H. A., Fritzson, P., and Vanrolleghem, P. A. (2007). Generating efficient executable models for complex virtual experimentation with the Tornado kernel. *Water Science and Technology* **56**, 65-73.

Crittenden, J. C., Hu, S. M., Hand, D. W., and Green, S. A. (1999). A kinetic model for H2O2/UV process in a completely mixed batch reactor. *Water Research* **33**, 2315-2328.

Einschlag, F. G., Feliz, M. R., and Capparelli, A. L. (1997). Effect of temperature on hydrogen peroxide photolysis in aqueous solutions. *Journal of Photochemistry and Photobiology a-Chemistry* **110**, 235-242.

Eriksen, T. E., Lind, J., and Merenyi, G. (1985). ON THE ACID-BASE EQUILIBRIUM OF THE CARBONATE RADICAL. *Radiation Physics and Chemistry* **26**, 197-199.

Fabian, I. (2006). Reactive intermediates in aqueous ozone decomposition: A mechanistic approach. *Pure and Applied Chemistry* **78**, 1559-1570.

Froment, G. F., and Bischoff, K. B. (1990). "Chemical Reactor Analysis and Design," 2/Ed. John Wiley & Sons, New York.

Glaze, W. H., Beltran, F., Tuhkanen, T., and Kang, J.-W. (1992). Chemical Models of Advanced Oxidation Processes. *Water Poll. Res. J. Canada* **27**, 23-42.

Glaze, W. H., Lay, Y., and Kang, J. W. (1995). ADVANCED OXIDATION PROCESSES - A KINETIC-MODEL FOR THE OXIDATION OF 1,2-DIBROMO-3-CHLOROPROPANE IN WATER BY THE COMBINATION OF HYDROGEN-PEROXIDE AND UV-RADIATION. *Industrial & Engineering Chemistry Research* **34**, 2314-2323.

Henze, M., Gujer, W., Mino, T., and van Loodsrecht, M. (2000). "Activated sludge models ASM1, ASM2, ASM2d and ASM3," IWA Publishing, London.

Hindmarsh, A. C., and Petzold, L. R. (1995). Algorithms and software for ordinary differential equations and differential-algebraic equations. *Computers in Physics* **9**, 148-155.

Hollender, J., Zimmermann, S. G., Koepke, S., Krauss, M., McArdell, C. S., Ort, C., Singer, H., von Gunten, U., and Siegrist, H. (2009). Elimination of Organic Micropollutants in a Municipal Wastewater Treatment Plant Upgraded with a Full-Scale Post-Ozonation Followed by Sand Filtration. *Environmental Science & Technology* **43**, 7862-7869.

Klassen, N. V., Marchington, D., and McGowan, H. C. E. (1994). H2O2 DETERMINATION BY THE I-3(-) METHOD AND BY KMNO4 TITRATION. *Analytical Chemistry* **66**, 2921-2925.

Kletting, P., and Glatting, G. (2009). Model selection for time-activity curves: the corrected Akaike information criterion and the F-test. *Z Med Phys* **19**, 200-6.

Kruithof, J. C., Kamp, P. C., and Martijn, B. J. (2007). UV/H2O2 treatment: A practical solution for organic contaminant control and primary disinfection. *Ozone-Science & Engineering* **29**, 273-280.

Li, K., Hokanson, D. R., Crittenden, J. C., Trussell, R. R., and Minakata, D. (2008). Evaluating UV/H2O2

processes for methyl tert-butyl ether and tertiary butyl alcohol removal: Effect of pretreatment options and light sources. *Water Research* **42**, 5045-5053.

Liao, C. H., and Gurol, M. D. (1995). CHEMICAL OXIDATION BY PHOTOLYTIC DECOMPOSITION OF HYDROGEN-PEROXIDE. *Environmental Science & Technology* **29**, 3007-3014.

Neta, P., Huie, R. E., and Ross, A. B. (1988). RATE CONSTANTS FOR REACTIONS OF INORGANIC RADICALS IN AQUEOUS-SOLUTION. *Journal of Physical and Chemical Reference Data* **17**, 1027-1284.

Parsons, S. A. (2004). "Advanced Oxidation Processes for Water and Wastewater Treatment," IWA Publishing, London.

Rosenfeldt, E. J., and Linden, K. G. (2004). Degradation of endocrine disrupting chemicals bisphenol A, ethinyl estradiol, and estradiol during UV photolysis and advanced oxidation processes. *Environmental Science & Technology* **38**, 5476-5483.

Sharpless, C. M., and Linden, K. G. (2003). Experimental and model comparisons of low- and medium-pressure Hg lamps for the direct and H2O2 assisted UV photodegradation of N-nitrosodimethylamine in simulated drinking water. *Environmental Science & Technology* **37**, 1933-1940.

Song, W., Ravindran, V., and Pirbazari, M. (2008). Process optimization using a kinetic model for the ultraviolet radiation-hydrogen peroxide decomposition of natural and synthetic organic compounds in groundwater. *Chemical Engineering Science* **63**, 3249-3270.

Standard Methods for the Examination of Water and Wastewater (1998). 20th edn, American Public Health Association Inc., New York.

Swaim, P., Royce, A., Smith, T., Maloney, T., Ehlen, D., and Carter, B. (2008). Effectiveness of UV advanced oxidation for destruction of micro-pollutants. *Ozone-Science & Engineering* **30**, 34-42.

von Gunten, U. (2003). Ozonation of drinking water: Part I. Oxidation kinetics and product formation. *Water Research* **37**, 1443-1467.

Weinstein, J., and Bielski, B. H. J. (1979). KINETICS OF THE INTERACTION OF HO2 AND O2-RADICALS WITH HYDROGEN-PEROXIDE - HABER-WEISS REACTION. *Journal of the American Chemical Society* **101**, 58-62.

Westerhoff, P., Aiken, G., Amy, G., and Debroux, J. (1999). Relationships between the structure of natural organic matter and its reactivity towards molecular ozone and hydroxyl radicals. *Water Research* **33**, 2265-2276.

Westerhoff, P., Song, R., Amy, G., and Minear, R. (1997). Applications of ozone decomposition models. *Ozone-Science & Engineering* **19**, 55-73.

Wu, C. L., and Linden, K. G. (2008). Degradation and byproduct formation of parathion in aqueous solutions by UV and UV/H2O2 treatment. *Water Research* **42**, 4780-4790.